A&A 373, 336–344 (2001)
DOI: 10.1051/0004-6361:20010499

Astronomy & Astrophysics

General relativistic satellite astrometry

II. Modeling parallax and proper motion

F. de Felice[1], B. Bucciarelli[2], M. G. Lattanzi[2], and A. Vecchiato[1]

[1] Istituto di Fisica "G. Galilei", Via Marzolo 1, 35100 Padova, Italy
e-mail: fernando.defelice@pd.infn.it; alberto.vecchiato@pd.infn.it
[2] Osservatorio Astronomico di Torino, Strada Osservatorio 20, 10025 Pino Torinese To, Italy
e-mail: bucc@to.astro.it

Received 24 March 2000 / Accepted 22 March 2001

Abstract. The non-perturbative general relativistic approach to global astrometry introduced by de Felice et al. (1998) is here extended to account for the star motions on the Schwarzschild celestial sphere. A new expression of the observables, i.e. angular distances among stars, is provided, which takes into account the effects of parallax and proper motions. This dynamical model is then tested on an end-to-end simulation of the global astrometry mission GAIA. The results confirm the findings of our earlier work, which applied to the case of a static (angular coordinates only) sphere. In particular, measurements of large arcs among stars (each measurement good to $\sim$100 μarcsec, as expected for $V \sim 17$ mag stars) repeated over an observing period comparable to the mission lifetime foreseen for GAIA, can be modeled to yield estimates of positions, parallaxes, and annual proper motions good to $\sim$15 μarcsec. This second round of experiments confirms, within the limitations of the simulation and the assumptions of the current relativistic model, that the space-born global astrometry initiated with Hipparcos can be pushed down to the 10^{-5} arcsec accuracy level proposed with the GAIA mission. Finally, the simplified case we have solved can be used as reference for testing the limiting behavior of more realistic models as they become available.

Key words. relativity – astrometry – methods: data analysis – space vehicles

1. Introduction

In a recent paper (de Felice et al. 1998) (Paper I from now on) a non-perturbative approach was developed to perform satellite astrometry in a general relativistic framework. We considered a background space-time geometry given by the Schwarzschild metric and modeled a *static* sphere centered at the Sun, i.e., stellar positions were defined by azimuths and colatitudes, only. This investigation into non-perturbative methods was stimulated by the high accuracy which can be reached by the forthcoming astrometric space-missions, for example GAIA, which is expected to measure positions, parallaxes and annual proper motions to better than 10 μarcsec for stars brighter than $V \sim 15$ mag. Non perturbative methods can, at least in principle, take into account the general relativistic effects with an approximation as high as is needed.

In this article, we complete the work we presented in Paper I by extending it to a dynamical simulation, in order to build a relativistic model which allows for the determination of parallaxes and proper motions. We use the same mathematical setup of Paper I.

Greek indices run from 0 to 3; subscript "i" marks a stellar position and the metric signature is taken +2; repeated indeces are to be summed over their range of values.

2. Mathematical preliminaries

We consider a mathematical model which consists of an astrometric satellite (the observer) orbiting on a spatially circular geodesic around the Sun. The latter is assumed non rotating, spherically symmetric and therefore generating a Schwarzschild space-time metric. As in Paper I, we neglect the contribution of the Earth and the other solar-system planets to the background geometry. Under these conditions, the center of the Sun coincides with the barycenter of the satellite-Sun system. Also, the space-time metric in polar coordinates is given by

$$\mathrm{d}s^2 = -\left(1-\frac{r_\mathrm{g}}{r}\right)\mathrm{d}t^2 + \frac{\mathrm{d}r^2}{\left(1-\frac{r_\mathrm{g}}{r}\right)} + r^2\left(\mathrm{d}\theta^2+\sin^2\theta\,\mathrm{d}\phi^2\right), \quad (1)$$

Send offprint requests to: M. G. Lattanzi,
e-mail: lattanzi@to.astro

where the colatitude $\theta \in [0, \pi]$, the azimuth $\phi \in [0, 2\pi]$ and the polar distance $r \in]0, \infty[$; $r_{\rm g} \equiv 2G\mathcal{M}_\odot/c^2$ is the gravitational radius of the Sun and $\mathcal{M}_\odot$ its mass (in conventional units). The observer's trajectory in the $\theta = \pi/2$ plane is given by the four-vector

$$u^\alpha = {\rm e}^\psi(\delta^\alpha_0 + \Omega\delta^\alpha_\phi) \tag{2}$$

where δ^β_α is the Kronecker delta, and

$${\rm e}^\psi = \left(1 - \frac{r_{\rm g}}{r} - \Omega^2 r^2\right)^{-1/2} \tag{3}$$

is the normalization factor (i.e., $u_\alpha u^\alpha = -1$), $\Omega = \pm(M/r^3)^{1/2}$ is the Keplerian angular velocity with respect to an observer at infinity and in units of $(\text{length})^{-1}$ ($M \equiv GM_\odot/c^2$).

A basic observable in astrometry is the angle between two stars. The cosine of such an angle is given by (Brumberg 1991):

$$\cos\psi_{12} = \frac{h_{\alpha\beta}k_1^\alpha k_2^\beta}{(h_{\rho\sigma}k_1^\rho k_1^\sigma)^{1/2}(h_{\iota\pi}k_2^\iota k_2^\pi)^{1/2}}, \tag{4}$$

where k_1^α and k_2^α are the components of the tangents to the null geodesics of the photons emitted by the two stars, and $h_{\alpha\beta} = g_{\alpha\beta} + u_\alpha u_\beta$ is a tensor which projects in the rest frame of the observer. The components of the null geodesics in the space-time defined by Eq. (1) are (de Felice & Clarke 1990)

$$k \equiv \begin{cases} k^0 = \left(1 - \dfrac{2M}{r}\right)^{-1} E_{\rm ph} \\ k^r = \pm\left[E^2_{\rm ph} - \dfrac{L^2_{\rm ph}}{r^2}\left(1 - \dfrac{2M}{r}\right)\right]^{1/2} \\ k^\theta = \pm\dfrac{1}{r^2}\left[L^2_{\rm ph} - \dfrac{l^2_{\rm ph}}{\sin^2\theta}\right]^{1/2} \\ k^\phi = \dfrac{1}{r^2\sin^2\theta} l_{\rm ph}, \end{cases} \tag{5}$$

where $E_{\rm ph}$ is the photon's total energy in units of c^2, $L_{\rm ph}$ and $l_{\rm ph}$ are respectively the total and the azimuthal angular momenta of the photons in units of c.

From Eqs. (1) and (5), and denoting $\Lambda \equiv L/E$ and $\lambda \equiv l/E$, Eq. (4) has the general form

$$\cos\psi_{12} = \Psi(\lambda_1, \lambda_2; \Lambda_1, \Lambda_2) \tag{6}$$

where Ψ is given by Eqs. (6) and (7) of Paper I (see also Appendix A of that paper). The linearized form of the observation Eq. (6) is then

$$-\sin\psi_{12}\delta\psi_{12} = \sum_{\mathcal{A}}[a_{\mathcal{A}}\delta\lambda_{\mathcal{A}} + b_{\mathcal{A}}\delta\Lambda_{\mathcal{A}}] \qquad \mathcal{A} = 1,\, 2 \tag{7}$$

where

$$a_{\mathcal{A}} = \frac{\partial\Psi}{\partial\lambda_{\mathcal{A}}}, \qquad b_{\mathcal{A}} = \frac{\partial\Psi}{\partial\Lambda_{\mathcal{A}}}.$$

The position of the observer is fixed once the radius of the orbit and the azimuthal angle $\phi_{\rm o}$ of the event of observation are given; the latter can be taken equal to zero, say, while the choice of the observer in the equatorial plane implies $\theta_{\rm o} = \pi/2$. The coordinate positions of the stars do not explicitly appear in Eqs. (6) and (7) since they are hidden in the constants of motion. However, the integration of the equations of motion (5) coupled with the observation Eq. (6), lead to relations which ultimately allow one to determine the unknown stellar positions.

2.1. The inclusion of parallax

In the simulation of a static sphere, the equations of motion of the photons were integrated assuming that distances from the Sun were infinitely large. In order to take into account finite coordinate distances to stars, we simply limit the integration of the radial equation accordingly. Therefore, we have

$$\int_r^{r_{\rm o}} \frac{{\rm sgn}(k^r)\,{\rm d}r'}{r'^2\sqrt{1 - \dfrac{\Lambda^2}{r'^2}\left(1 - \dfrac{2M}{r'}\right)}} = \int_\theta^{\pi/2} \frac{{\rm sgn}(k^\theta)\sin\theta'\,{\rm d}\theta'}{\sqrt{\Lambda^2\sin^2\theta' - \lambda^2}}, \tag{8}$$

and

$$\int_\theta^{\pi/2} \frac{{\rm sgn}(k^\theta)\lambda\,{\rm d}\theta'}{\sin\theta'\sqrt{\Lambda^2\sin^2\theta' - \lambda^2}} = \int_\phi^{\phi_{\rm o}} {\rm d}\phi', \tag{9}$$

where $(r,\, \theta,\, \phi)$ specify the coordinate position of a star whose photons are received by the observer at $(r_{\rm o},\, \theta_{\rm o} = \pi/2,\, \phi_{\rm o})$.

The constant of motion Λ can be expressed in terms of the distance, $r_{\rm c}$, of the point of closest approach of the photon's trajectory to the Sun. At such point $k^r = 0$ and therefore

$$\Lambda^2 = r_{\rm c}^2\left(1 - \frac{r_{\rm g}}{r_{\rm c}}\right)^{-1} \equiv w^2(r_{\rm c}). \tag{10}$$

The plot of the function $w^2(r_{\rm c})$ has a minimum at $r_{\rm c} = 3M$. As the radius of the Sun $R_\odot$ is much bigger than $3M$, in practice only two cases need to be considered: $r_{\rm c} > R_\odot$ and $r_{\rm c} \le R_\odot$.

For $r_{\rm c} > R_\odot$, there are no restrictions to the access of directions on the sky, as the emitted photons can always reach the observer regardless of the relative location of the Sun. In this case the integration of Eqs. (8) and (9) yields relations of the type

$$\begin{cases} z(r, r_{\rm c}) \;=\; g(\theta, \phi; \phi_{\rm o}) \\ \dfrac{\lambda^2}{\Lambda^2} \;=\; h(\theta, \phi; \phi_{\rm o}) \qquad\qquad r_{\rm c} > R_\odot. \\ \Lambda \;=\; w(r_{\rm c}) \end{cases} \tag{11}$$

For $r_c \leq R_\odot$, the only meaningful cases are those with the satellite-based observer between the Sun and the star. In this configuration only two relations are used, i.e.

$$\begin{cases} \tilde{z}(r,\Lambda) = g(\theta,\phi;\phi_o) \\ \dfrac{\lambda^2}{\Lambda^2} = h(\theta,\phi;\phi_o) \end{cases} \qquad r_c \leq R_\odot. \tag{12}$$

Functions $g(\theta, \phi; \phi_o)$, $h(\theta, \phi; \phi_o)$ and $w(r_c)$ are unchanged from Paper I (see Appendix A there), while $z(r, r_c)$ and $\tilde{z}(r, \Lambda)$ now read

$$\begin{aligned} z(r,r_c) = {} & \mathrm{flag}_2\left(1-\frac{2M}{r_c}\right)^{-1/2}\left\{\left(1-\frac{M}{r_c}\right)\left(\arcsin\frac{r_c}{r_o}\right.\right. \\ & \left.-\arcsin\frac{r_c}{r}-\mathrm{flag}_1\pi\right) \\ & -\frac{M}{r_c}\left[\left(\frac{r_c}{r_o}+2\right)\sqrt{\frac{r_o-r_c}{r_o+r_c}}\right. \\ & \left.\left.-\mathrm{flag}_2\left(\frac{r_c}{r}+2\right)\sqrt{\frac{r-r_c}{r+r_c}}\right]\right\}, \end{aligned} \tag{13}$$

$$\begin{aligned} \tilde{z}(r,\Lambda) = {} & \left(\frac{1}{6r_o^3}-\frac{1}{6r^3}-\frac{M}{4r_o^4}+\frac{M}{4r^4}\right)c^3\Lambda^3 \\ & +\left(\frac{1}{r_o}-\frac{1}{r}\right)c\Lambda. \end{aligned} \tag{14}$$

We use the expression $p \equiv r_o/r$ to define the coordinate parallax, and transform Eqs. (11) through (14) accordingly. In our model, r_o is the distance of the observer to the Sun, and if $r_o = 1$ AU, the above definition is close to the one used in classical astrometry ($p = \sin^{-1}(r_o/r) \simeq r_o/r$.

With this substitution, the functions $z(r, r_c)$ and $\tilde{z}(r, \Lambda)$ in (11) and (12) are replaced by the following expressions:

$$\begin{aligned} f(p,r_c) = {} & \mathrm{flag}_2\left(1-\frac{2M}{r_c}\right)^{-1/2}\left\{\left(1-\frac{M}{r_c}\right)\left(\arcsin\frac{r_c}{r_o}\right.\right. \\ & \left.-\arcsin\frac{pr_c}{r_o}-\mathrm{flag}_1\pi\right) \\ & -\frac{M}{r_c}\left[\left(\frac{r_c}{r_o}+2\right)\sqrt{\frac{r_o-r_c}{r_o+r_c}}\right. \\ & \left.\left.-\mathrm{flag}_2\left(\frac{pr_c}{r_o}+2\right)\sqrt{\frac{r_o-pr_c}{r_o+pr_c}}\right]\right\}, \end{aligned} \tag{15}$$

$$\begin{aligned} \tilde{f}(p,\Lambda) = {} & \left(\frac{1}{6r_o^3}-\frac{p^3}{6r_o^3}-\frac{M}{4r_o^4}+\frac{Mp^4}{4r_o^4}\right)c^3\Lambda^3 \\ & +\left(\frac{1}{r_o}-\frac{p}{r_o}\right)c\Lambda. \end{aligned} \tag{16}$$

Then, the differential observation Eq. (7) can be cast into a form containing the differentials of the astrometric quantities θ, ϕ, and p by means of the expressions:

$$\mathrm{d}\Lambda = \alpha_\Lambda\,\mathrm{d}\theta + \beta_\Lambda\,\mathrm{d}\phi + \gamma_\Lambda\,\mathrm{d}p, \tag{17}$$

$$\mathrm{d}\lambda = \alpha_\lambda\,\mathrm{d}\theta + \beta_\lambda\,\mathrm{d}\phi + \gamma_\lambda\,\mathrm{d}p. \tag{18}$$

Let us consider the cases of Eqs. (11) and (12) separately:

- $r_c > R_\odot$ – A variation in angular position implies a variation of λ and Λ. This, in turn, implies a variation of r_c from Eq. (10). After some algebra, we derive the following coefficients:

$$\begin{aligned} \alpha_\Lambda &= \frac{\partial w}{\partial r_c}\left(\frac{\partial f}{\partial r_c}\right)^{-1}\frac{\partial g}{\partial\theta} \\ \beta_\Lambda &= \frac{\partial w}{\partial r_c}\left(\frac{\partial f}{\partial r_c}\right)^{-1}\frac{\partial g}{\partial\phi} \\ \gamma_\Lambda &= -\frac{\partial w}{\partial r_c}\left(\frac{\partial f}{\partial r_c}\right)^{-1}\frac{\partial f}{\partial p} \end{aligned} \tag{19}$$

$$\begin{aligned} \alpha_\lambda &= \frac{\Lambda^2}{2\lambda}\frac{\partial h}{\partial\theta}+\frac{\lambda}{\Lambda}\frac{\partial w}{\partial r_c}\left(\frac{\partial f}{\partial r_c}\right)^{-1}\frac{\partial g}{\partial\theta} \\ \beta_\lambda &= \frac{\Lambda^2}{2\lambda}\frac{\partial h}{\partial\phi}+\frac{\lambda}{\Lambda}\frac{\partial w}{\partial r_c}\left(\frac{\partial f}{\partial r_c}\right)^{-1}\frac{\partial g}{\partial\phi} \\ \gamma_\lambda &= -\frac{\lambda}{\Lambda}\frac{\partial w}{\partial r_c}\left(\frac{\partial f}{\partial r_c}\right)^{-1}\frac{\partial f}{\partial p}. \end{aligned} \tag{20}$$

The partial derivatives of f which enter Eqs. (17) and (18) differ from their analogues in Paper I (see Appendix A of that paper) and read:

$$\begin{aligned} \frac{\partial f}{\partial r_c} = {} & -\left(1-\frac{2M}{r_c}\right)^{-1}\frac{M}{r_c^2}f(p,r_c)+\mathrm{flag2}\left(1-\frac{r_g}{r_c}\right)^{-1/2} \\ & \times\left\{\frac{M}{r_c^2}\left(\arcsin\frac{r_c}{r_o}-\mathrm{flag2}\arcsin\frac{pr_c}{r_o}-\mathrm{flag1}\pi\right)\right. \\ & +\left(1-\frac{M}{r_c}\right)\left[\left(1-\frac{r_c^2}{r_o^2}\right)^{-1/2}\frac{1}{r_o}-\mathrm{flag2}\left(1-\frac{p^2r_c^2}{r_o^2}\right)^{-1/2}\frac{p}{r_o}\right] \\ & +\frac{M}{r_c^2}\left[\left(\frac{r_c}{r_o}+2\right)\sqrt{\frac{r_o-r_c}{r_o+r_c}}-\mathrm{flag2}\left(\frac{pr_c}{r_o}+2\right)\sqrt{\frac{r_o-pr_c}{r_o+pr_c}}\right] \\ & -\frac{M}{r_c}\left[\frac{1}{r_o}\sqrt{\frac{r_o-r_c}{r_o+r_c}}-\left(\frac{r_c}{r_o}+2\right)\frac{r_o}{(r_o+r_c)^2}\sqrt{\frac{r_o+r_c}{r_o-r_c}}\right. \\ & \quad -\mathrm{flag2}\frac{p}{r_o}\sqrt{\frac{r_o-pr_c}{r_o+pr_c}}+\mathrm{flag2}\left(\frac{pr_c}{r_o}+2\right) \\ & \left.\left.\quad\times\frac{pr_o}{(r_o+pr_c)^2}\sqrt{\frac{r_o+pr_c}{r_o-pr_c}}\right]\right\}, \end{aligned} \tag{21}$$

$$\frac{\partial f}{\partial p} = -\left(1-\frac{2M}{r_\mathrm{c}}\right)^{-1/2}\left\{\left(1-\frac{M}{r_\mathrm{c}}\right)\times\right.$$
$$\left(1-\frac{p^2r_\mathrm{c}^2}{r_\mathrm{o}^2}\right)^{-1/2}\frac{r_\mathrm{c}}{r_\mathrm{o}}-\frac{M}{r_\mathrm{c}}\left[\frac{r_\mathrm{c}}{r_\mathrm{o}}\sqrt{\frac{r_\mathrm{o}-pr_\mathrm{c}}{r_\mathrm{o}+pr_\mathrm{c}}}-\right.$$
$$\left.\left.\left(\frac{pr_\mathrm{c}}{r_\mathrm{o}}+2\right)\frac{r_\mathrm{c}r_\mathrm{o}}{(r_\mathrm{o}+pr_\mathrm{c})^2}\sqrt{\frac{r_\mathrm{o}+pr_\mathrm{c}}{r_\mathrm{o}-pr_\mathrm{c}}}\right]\right\}. \quad (22)$$

- $r_\mathrm{c}\le R_\odot$ – Following the same arguments as before we obtain the new coefficients:

$$\alpha_\Lambda = \left(\frac{\partial\tilde f}{\partial\Lambda}\right)^{-1}\frac{\partial g}{\partial\theta}$$
$$\beta_\Lambda = \left(\frac{\partial\tilde f}{\partial\Lambda}\right)^{-1}\frac{\partial g}{\partial\phi} \quad (23)$$
$$\gamma_\Lambda = -\left(\frac{\partial\tilde f}{\partial\Lambda}\right)^{-1}\frac{\partial\tilde f}{\partial p}$$
$$\alpha_\lambda = \frac{\Lambda^2}{2\lambda}\frac{\partial h}{\partial\theta_i}+\frac{\lambda}{\Lambda}\left(\frac{\partial\tilde f}{\partial\Lambda}\right)^{-1}\frac{\partial g}{\partial\theta}$$
$$\beta_\lambda = \frac{\Lambda^2}{2\lambda}\frac{\partial h}{\partial\phi}+\frac{\lambda}{\Lambda}\left(\frac{\partial\tilde f}{\partial\Lambda}\right)^{-1}\frac{\partial g}{\partial\phi} \quad (24)$$
$$\gamma_\lambda = -\frac{\lambda}{\Lambda}\left(\frac{\partial\tilde f}{\partial\Lambda}\right)^{-1}\frac{\partial\tilde f}{\partial p},$$

where the following expressions differ from the analogue relations used for the static case:

$$\frac{\partial\tilde f}{\partial\Lambda} = 3\left(\frac{1}{6r_\mathrm{o}^3}-\frac{p^3}{6r_\mathrm{o}^3}-\frac{M}{4r_\mathrm{o}^4}+\frac{Mp^4}{4r_\mathrm{o}^4}\right)c^3\Lambda^2+$$
$$\left(\frac{1}{r_\mathrm{o}}-\frac{p}{r_\mathrm{o}}\right)c, \quad (25)$$

$$\frac{\partial\tilde f}{\partial p} = \left(\frac{Mp^3}{r_\mathrm{o}^4}-\frac{p^2}{2r_\mathrm{o}^3}\right)c^3\Lambda^3-\frac{c\Lambda}{r_\mathrm{o}}. \quad (26)$$

2.2. Mathematical description of stellar motion

The motion of a distant star can be formally described by considering its Schwarzschild coordinates functions of coordinate time. Replacing these functions with their Taylor expansions, one has

$$\begin{cases} p(t) = p(t_0)+\dot p\times(t-t_0)+\\ \qquad 0.5\,\ddot p\times(t-t_0)^2+...\\ \theta(t) = \theta(t_0)+\mu_\theta\times(t-t_0)+\\ \qquad 0.5\,\dot\mu_\theta\times(t-t_0)^2+...\\ \phi(t) = \phi(t_0)+\mu_\phi\times(t-t_0)+\\ \qquad 0.5\,\dot\mu_\phi\times(t-t_0)^2+..., \end{cases} \quad (27)$$

where we made use of the definition of coordinate parallax, $p(t)=r_\mathrm{o}/r(t)$, introduced earlier, and of the definitions $\mu_\theta\equiv\frac{\mathrm{d}\theta}{\mathrm{d}t}$, $\mu_\phi\equiv\frac{\mathrm{d}\phi}{\mathrm{d}t}$, which we will refer to as (angular) proper motions. Also, the time derivative of p in Eqs. (27) can be written as $\dot p=-\frac{p^2}{r_\mathrm{o}}V_\mathrm{r}$, where $V_\mathrm{r}\equiv\frac{\mathrm{d}r}{\mathrm{d}t}$ is the coordinate radial velocity. We recall here that the coordinate quantities in Eqs. (27) are not directly observable. However, as $r\gg r_\mathrm{o}$, $p(t_0)$, $\theta(t_0)$, $\phi(t_0)$, $\dot p$ (or V_r), μ_θ, and μ_ϕ can be interpreted as the corresponding quantities of classical astrometry.

The effects of a variable coordinate parallax on our relativistic model are fully taken into account by *a)* inserting the expression for $p(t)$ in Eqs. (27), truncated to the required order, in the formulas derived in the previous section and defining the coefficients γ_Λ and γ_λ in Eqs. (17) and (18), and by *b)* substituting the variation of the coordinate parallax $p(t)$, i.e. $\delta p(t)=\delta p(t_0)+\delta\dot p\times(t-t_0)+0.5\,\delta\ddot p\times(t-t_0)^2+...$, again in Eqs. (17) and (18)[1].

Similar considerations hold for the angular quantities in Eqs. (27), i.e., the relativistic model can be specialized to take into account the time variability of the angular coordinates with no restrictions on which terms of their Taylor expansion can be included. The choice of which terms to include will depend not only on the distance to the objects and how fast they move on the Schwarzschild sphere, as it would be for single stars, but also on their nature (binary, variable, presence of unseen low-mass companions, etc.). In this article all of our objects are assumed single stars, i.e., point like sources of constant luminosity[2].

For simplicity, we decided to adopt the basic model

$$\begin{cases} p(t) = p(t_0)\\ \theta(t) = \theta(t_0)+\mu_\theta\times(t-t_0)\\ \phi(t) = \phi(t_0)+\mu_\phi\times(t-t_0), \end{cases} \quad (28)$$

[1] As in Paper I, the small differences $\delta p(t_0)$, $\delta\dot p$, etc. are intended relative to the approximate (initial) values of a suitable reference catalog.

[2] This is similar to what was done for the Hipparcos mission. There, the Sphere Solution, i.e., the high accuracy reconstruction of the celestial sphere, was performed on a subset of the program sources called "primary" (single and non-variable) stars, for which the only non-secular component of their motion is the parallactic displacement.

and in the remainder of this section we briefly discuss the implications of this choice.

In principle, it is possible to deduce all of the components of stellar velocity by utilizing astrometric measurements only. In particular, the radial velocity of a star affects both its distance (i.e., *parallax*, see the expression for $\dot{p}$ given above) and its angular (i.e., *proper*) motion; therefore, it is necessary to evaluate whether such effects need to be included in the model. Straightforward calculations show that a Δp of $\sim$10 μarcsec in 5 years, which we can assume as representative of the minimum variation measurable by a GAIA-like mission, requires a radial velocity of $V_{\rm r} \sim 1.8 \times 10^4$ km s^{-1} at a distance of 100 pc. Therefore, this is probably a negligible effect for the great majority of the potential targets.

The annual proper motion variation (in arcsec/yr^2) induced by stellar radial velocity, in astrometric jargon *perspective acceleration* (or *foreshortening term*), is estimated by the expression

$$\dot{\mu}\ (\text{arcsec/yr}^2) \simeq -0.1 V_{\rm r} V_{\rm t} p^2 \cdot \sin 1''$$

(Green 1985; Bucciarelli et al. 1995), where p is given in arcsec, $V_{\rm r}$ and $V_{\rm t}$ (the tangential velocity) in Km s^{-1}, and $\sin 1''$ is the conversion factor from arcsec to radians. For example, a star with $V_{\rm r} = V_{\rm t} = 100$ Km s^{-1} at a distance of $\gtrsim$80 pc will have a displacement $\lesssim$10 μarcsec after 5 years.

Another effect induced by $V_{\rm r}$ ($\propto \dot{p}$) is an *apparent place* effect, since it represents the change in the star position as seen from Earth. The yearly angular variation amounts to approximately

$$\frac{p^2 V_{\rm r} \cdot \sin u}{\sin 1''} \quad (\text{arcsec}),$$

where p is given in radians, $V_{\rm r}$ in AU/yr, and u is the angle between the observer and the star as seen from the Sun[3]. Using the same value of the radial velocity as before (which corresponds to $\sim$15 AU/yr), this term will add less than $\sim$1 μarcsec to the 5-year positional change of all targets beyond $\sim$20 pc; therefore, it appears negligible in virtually all cases.

From the above considerations, the choice of model (28) appears appropriate for describing the effects of stellar motions for the large majority of the single stars accessible to GAIA. Nonetheless, for a non-negligible fraction of stars in the solar neighborhood, higher order terms will have to be introduced thus providing estimates of *astrometric* radial velocities.

[3] Notice that, even though in our relativistic formulation the star's coordinates are naturally given in the barycentric reference frame, any stellar intrinsic motion which would cause a change in the *observed* directions to the star has to be included in the model in order not to bias the estimate of the *actual*, i.e. barycentric, directions.

2.3. The inclusion of proper motion

The addition of the two components of proper motion to our unknowns is rather straightforward, the difference being the integration limits in Eqs. (8) and (9) are now functions of coordinate time, $\theta(t)$ and $\phi(t)$.

The system of Eqs. (12) in Paper I (with the inclusion of the parallax as shown in the previous section) becomes

$$\begin{cases} f(p, r_{\rm c}) = g\,(\theta(t_0) + \mu_\theta(t-t_0), \\ \qquad\qquad \phi(t_0) + \mu_\phi(t-t_0); \phi_{\rm o}) \\ \dfrac{\lambda^2(\tau)}{\Lambda^2(\tau)} = h\,(\theta(t_0) + \mu_\theta(t-t_0), \\ \qquad\qquad \phi(t_0) + \mu_\phi(t-t_0); \phi_{\rm o}) \\ \Lambda(\tau) = w(r_{\rm c}). \end{cases} \tag{29}$$

System (29) is formally identical to Eqs. (11) except for the time dependence which allows for inclusion of proper motion as a correction term in a Taylor expansion of the corresponding angular coordinate. Then the differential relations between the constants of motion Λ and λ, and the unknowns will be formally the same as in (17) and (18), that is

$$\delta\Lambda = \alpha_\Lambda \delta\theta(t) + \beta_\Lambda \delta\phi(t) + \gamma_\Lambda \delta p, \tag{30}$$

$$\delta\lambda = \alpha_\lambda \delta\theta(t) + \beta_\lambda \delta\phi(t) + \gamma_\lambda \delta p. \tag{31}$$

Since it is

$$g(\theta(t_0),\ \phi(t_0)\ , \mu_\theta, \mu_\phi) = g(\theta(t_0) + \mu_\theta(t-t_0), \phi(t_0) + \mu_\phi(t-t_0))$$

and

$$h(\theta(t_0),\ \phi(t_0)\ , \mu_\theta, \mu_\phi) = h(\theta(t_0) + \mu_\theta(t-t_0), \phi(t_0) + \mu_\phi(t-t_0)),$$

we finally obtain

$$\begin{aligned} -\sin\psi_{12}(t)\ \delta\psi_{12} = {} & A_1\,\delta\theta_1(t_0) + B_1\,\delta\phi_1(t_0) + \\ & C_1\,\delta r_1 + D_1\,\delta\mu_{\theta_1} + E_1\,\delta\mu_{\phi_1} + \\ & A_2\,\delta\theta_2(t_0) + B_2\,\delta\phi_2(t_0) + \\ & C_2\,\delta r_2 + D_2\,\delta\mu_{\theta_2} + E_2\,\delta\mu_{\phi_2}, \end{aligned} \tag{32}$$

where

$$\begin{aligned} &A_1 = a_1\alpha_{\lambda_1} + b_1\alpha_{\Lambda_1},\ A_2 = a_2\alpha_{\lambda_2} + b_2\alpha_{\Lambda_2}, \\ &B_1 = a_1\beta_{\lambda_1} + b_1\beta_{\Lambda_1},\ B_2 = a_2\beta_{\lambda_2} + b_2\beta_{\Lambda_2}, \\ &C_1 = a_1\gamma_{\lambda_1} + b_1\gamma_{\Lambda_1},\ C_2 = a_2\gamma_{\lambda_2} + b_2\gamma_{\Lambda_2}, \\ &D_1 = A_1(t-t_0), \qquad D_2 = A_2(t-t_0), \\ &E_1 = B_1(t-t_0), \qquad E_2 = B_2(t-t_0). \end{aligned} \tag{33}$$

The coefficients of the linearized condition Eq. (32) are calculated using the catalog values of the relevant quantities. The adjustments $\delta\theta(t_0)$, $\delta\phi(t_0)$, $\delta p(t_0)$, $\delta\mu_\theta$, and $\delta\mu_\phi$ represent the unknown quantities needed to bring the catalog values closer to the true ones. Finally, $\sin\psi\ \delta\psi$ is the linearized form of the GAIA observation; again, the numerical values for $\sin\psi$ are derived from the catalog values, whereas $\delta\psi$ is the difference between the angular distance measured by the satellite (which is within 100 μarcsec of the true distance) and the corresponding catalog-derived quantity.

Although the proper motion listed in our simulated catalog is the variation of the stellar coordinates with respect to the *coordinate* time, in the simulation we have to refer to the satellite proper-time τ. The latter therefore has to be converted into coordinate time in order to compute the correct stellar position.

The relation between coordinate time and proper-time of the orbiting observer is given by

$$\mathrm{d}\tau = \mathrm{e}^{-\psi}\,\mathrm{d}t = \sqrt{1-\frac{3M}{r_\mathrm{o}}}\,\mathrm{d}t. \tag{34}$$

Here we have always assumed $\tau = 0$ for $t = 0$, so that

$$\tau = \sqrt{1-\frac{3M}{r_\mathrm{o}}}t. \tag{35}$$

3. End-to-end simulation

The simulation of the dynamical case follows the same three-step procedure utilized for the static one, with the appropriate changes due to the inclusion of the new variables, parallax and proper motions.

First, we generate the set of *true* quantities, which define initial location and temporal evolution of the stellar positions on the relativistic (Schwarzschild) sphere, according to the basic model (i.e., Eq. (28)).

Stars are generated within a uniform density sphere of 500 pc centered on the Sun (i.e., $p \geq 2$ mas), the individual proper motions are computed assuming a linear velocity dispersion of $\sigma_v = 15$ km s^{-1}, while radial velocity has been neglected. The distribution and kinematics of the resulting sample of simulated stars is not representative of the motions of the corresponding (relatively) small portion of the actual Galaxy. Neverthless, the adopted values are adequate, within the scope of this work, for the generation of realistic angular motions.

The corresponding *catalog* values are generated, as usual, by adding suitable root-mean-square (rms) errors to the true values (see Table 1)

Next, we find the stellar pairs which can be observed by a satellite that sweeps the sky following a Hipparcos-like scanning law. The result of these two steps is the generation of the measured quantity, $-\sin\psi(t)\delta\psi$, and of the coefficients in Eq. (32) for the construction of the linearized condition equations for all of the observed pairs. Finally, the least-squares solution of the system is found by means of a conjugate-gradient method, suitable for large and sparse matrices like ours, and the adjustment errors are directly computed by comparison to the true values.

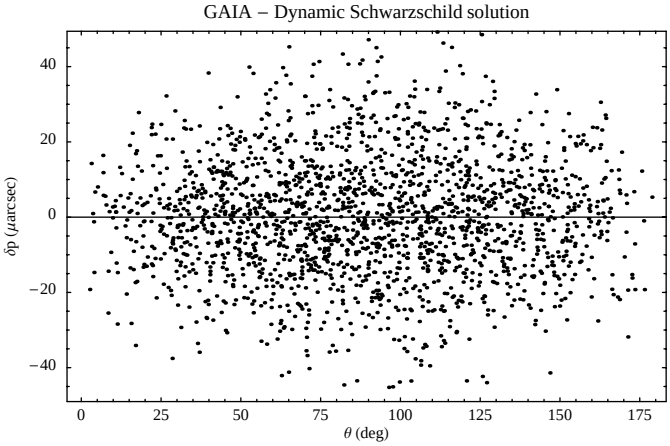

Fig. 1. *True* parallax errors versus colatitude (θ). Here and in the following graphics outliers are not considered.

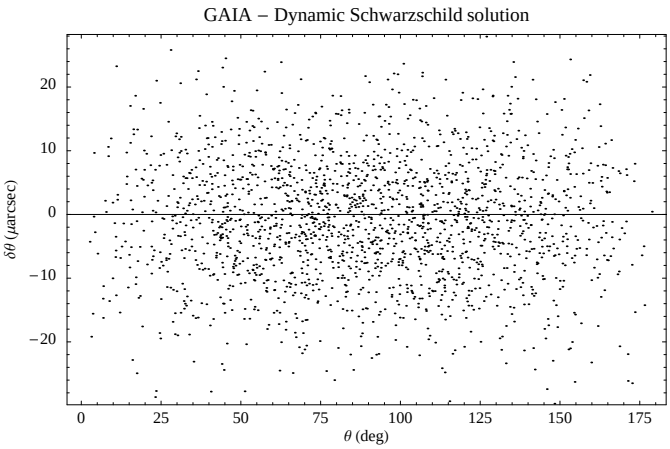

Fig. 2. *True* colatitude errors versus colatitude.

In Table 1, the values of the parameters in common with the static simulation are unchanged from those adopted in Paper I; this to keep maximum consistency with the static treatment, albeit GAIA's baseline configuration has changed in the meantime (see next section).

4. Results and discussion

Table 2 shows the typical results of the simulation of 5 different classes of the dynamical model. The mission is always started at $t = -T/2$, while its length varies from 2 to 5 years. The catalog reference (mean) time is always at half the mission lifetime ($t = T/2$), which provides the most accurate positions, while the correlation between position and proper motion is minimized (Eichhorn 1969; Mignard et al. 1985).

Figures 1–5 show the results for the 5-year-period case. Plotted are the *true* errors (i.e., the individual differences between estimated and true values) of the five astrometric parameters considered versus co-latitude.

Table 1. Most relevant parameters of the GAIA dynamic simulation.

parameter	*numerical value*	*comment*
orbital radius	1.496×10^{11} m	same as Earth's orbital radius ($R_\oplus$)
precession angle	43°	same as solar aspect angle
satellite spin period	128 min	
angles between three viewing directions	54°, 78°.5	Only two viewing directions retained in latest designs
field-of-view of each telescope	1°.6	
mission duration (T)	up to 5 years	
mission starting time (t_0)	$-T/2$	minimum correlation between coords. and proper motions
No. of simulated stars	2000	same magnitude ($V \sim 17$ mag)
No. of unknowns	up to 10 000	up to five parameters per stars
radius of the simulated sphere	2 mas	uniform density sphere of 500 pc in radius
assumed velocity distribution	15 km s^{-1}	for the simulation of proper motions
catalog error on coordinates and parallax	2 mas	
catalog error on proper motions	2 mas/year	
single-measurement error ($\sigma_{\rm oss}$)	100 μarcsec	as expected for pairs of $V \sim 17$ mag stars

Table 2. Results of a set of simulations with $T = 2$ to 5 years and $t_0 = -T/2$. Columns labelled with "n.it." and "$n_{\rm obs}$" are the number of iterations needed for convergence (5000 was the maximum number of iterations allowed) and the number of arcs observed during the simulation, respectively; Q is the equations-to-unknowns ratio, and $\langle \delta x \rangle$ and $\sigma_{\delta x}$ refer to the mean and standard deviation of the true errors of the least-squares solution for the variable x.

T	n.it.	$n_{\rm obs}$	Q	$\langle \delta p \rangle$	$\sigma_{\delta p}$	$\langle \delta\theta \rangle$	$\sigma_{\delta\theta}$	$\langle \sin\theta\, \delta\phi \rangle$	$\sigma_{\sin\theta\,\delta\phi}$	$\langle \delta\mu_\theta \rangle$	$\sigma_{\delta\mu_\theta}$	$\langle \sin\theta\, \delta\mu_\phi \rangle$	$\sigma_{\sin\theta\,\delta\mu_\phi}$
(yr)				(μas)	(μas)	(μas)	(μas)	(μas)	(μas)	(μas/yr)	(μas/yr)	(μas/yr)	(μas/yr)
5	83	286431	28.6	0.20	15.79	−0.86	9.49	−0.06	13.54	−0.02	6.58	−0.34	7.84
4	99	227869	22.8	0.20	17.88	−0.19	10.67	0.53	15.28	0.60	9.60	−0.89	11.31
3	124	172150	17.2	0.29	20.73	−0.76	12.97	−1.03	17.88	−0.13	15.65	1.72	19.34
2.5	172	144063	14.4	0.28	22.98	−0.89	15.56	−2.71	19.91	−0.18	21.52	3.31	25.32
2	839	115218	11.5	0.58	29.75	−0.83	21.06	3.67	26.64	0.45	67.32	−4.98	52.69

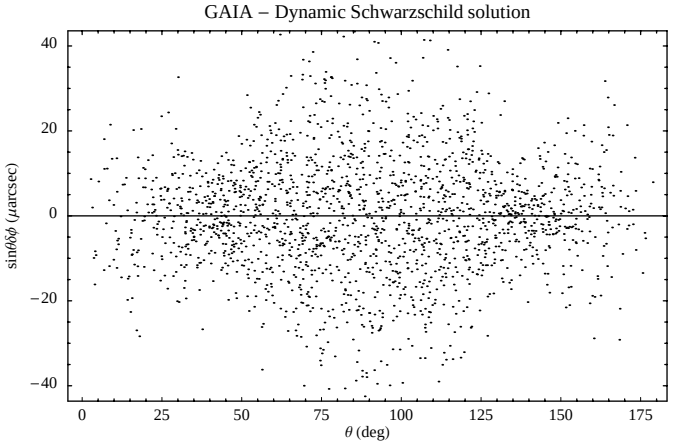

Fig. 3. *True* longitude errors versus colatitude. Notice the errors become smaller near the colatidudes 43° and 137°. This is where the number of connections (observations) per stars peaks as a result of the particular sky coverage startegy simulated.

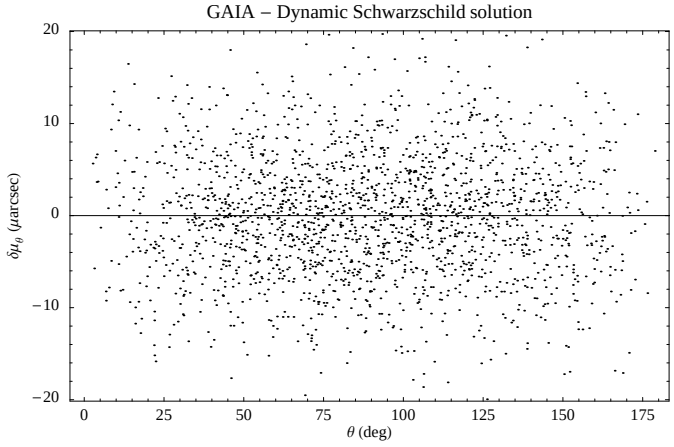

Fig. 4. *True* colatitude proper motion errors versus colatitude.

Similarly to the static solutions, the errors reach their minimum values near colatitudes 43° and 137°, where the number of connections (observations) per star peaks as a result of the sky coverage imposed by the sky scanning strategy adopted. The effect is particularly evident for the two longitudinal unknowns $\sin\theta\ \delta\phi$ and the corresponding proper motion component $\sin\theta\ \delta\mu_\phi$. Moreover, the errors compare well with the approximation (valid in the absence of correlation among the observations) $\sigma_{\rm oss}/\sqrt{Q}$, where Q is the average number of equations per unknown (see

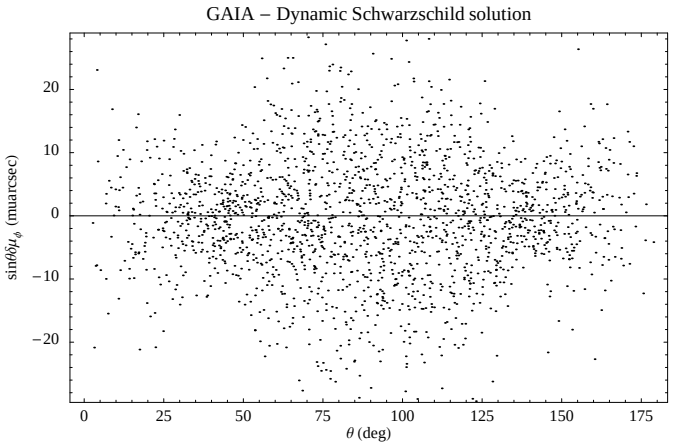

Fig. 5. *True* longitude proper motion errors versus colatitude.

Table 2) and $\sigma_{\rm oss} = 100$ μarcsec, for the average measurement error. This is true for all but the simulation with $T =$ 2 year, for which the proper motion errors are $\sim$2 times larger than the expected value of $\sim$30 μarcsec. This suggests that the 5-parameter dynamical model becomes inadequate as the relatively short time baseline makes it difficult to disentangle the secular (proper motion) component of stellar motions from the quadratic (parallax) one. Experiments run with $T = 1.5$ year and $T =$ 1 year failed to produce meaningful solutions. Therefore, it appears that a fully dynamical solution has to wait for $\sim$2 years of uninterrupted observations before being attempted, a result consistent with earlier findings from preparatory studies for the Hipparcos mission.

Consistent with the results presented in Paper I is also the finding that the error in longitude is larger than that in latitude. This is again an effect of the scanning law, and theoretical predictions (Betti & Sansò 1985) anticipates $\sigma_{\sin\theta\,\delta\phi}/\sigma_{\delta\theta} \sim 1.6$. This value compares well with the ratio of $\simeq$1.4 derived from the results of the 5-year-mission case in Table 2. Notice that the effect is significantly less pronounced ($\simeq$1.2) for the two components of proper motion.

4.1. Rank deficiency

With the addition of the kinematical parameters the rank deficiency of the design matrix of the observation equations increases. For a classical sphere model (as in Hipparcos) the design matrix has a rank deficiency of 6, twice that of the static case (Paper I). In our case, rank deficiency is probably less, as the formulation of the relativistic model requires to specify the trajectory of the observer, i.e., a circular orbit in the plane $\theta_{\rm o} = \pi/2$. Nevertheless, the numerical method we used for solving the system of equations can deal with rank deficient matrices without the addition of external constraints otherwise necessary to find the least-squares solution among the infinite possible ones, i.e., to lock the solution in a given system of coordinates (see discussion in Paper I). To investigate the statistical properties of the unconstrained solutions, we ran the 5-year case with different sets of constraint equations. The generic form of any of such equations (each added to the system of equations with "infinite" weight) is

$$\delta(unk) = unk(true) - unk(catalog),$$

where $\delta(unk)$ is the correction to any of the unknowns $\delta\theta$, $\delta\phi$, $\delta\mu_\theta$, and $\delta\mu_\phi$[4]. In this form, the constraint equations fix the values of the astrometric parameters of selected stars to their true values ($unk(true)$), which are always available in a simulation. Therefore, compensation for rank deficiency is done through the best possible information. Up to 6 of such equations are used, in which case 4 of them are relative to one star and the remaining 2 are for a second star suitably located on the Schwarzschild sphere. The results show that the errors of the constrained solutions are indistinguishable from those in Table 2. The same conclusion holds for the average values of the true errors $\langle\delta\theta\rangle$, $\langle\delta\phi, \sin\theta\rangle$, $\langle\delta\mu_\theta\rangle$, and $\langle\delta\mu_\phi, \sin\theta\rangle$ of the constrained solutions, they all have the sub-μarcsec values of the corresponding quantities in Table 2. This, in turn, suggests that the coordinate frame of the reconstructed spheres were always close to the Schwarzschild sphere defined by the true coordinates.

Issues related to rank deficiency of the GAIA sphere will have to be addressed in detail once a more advanced relativistic model[5] becomes available.

4.2. Catalog errors

A set of experiments was devoted to investigating the effect of increasing catalog errors on the sphere solutions. The true values of positions, parallax, and proper motions were degraded with different catalog errors in the range 1$\div$1200 mas (or mas/yr). As usual, the quality of the adjusted parameters of any of the solutions was gauged by calculating mean and standard deviation of the corresponding true errors. The solutions corresponding to catalog errors from 1 to 5 mas do not show appreciable differences. Then, the standard deviations begin to increase monotonically, but the numbers remain below 10% of the best value for catalog errors of up to 200 mas. The mean values do not manifest a similar monotonic increase, and stay stationary at 1–2 μarcsec

4.3. Compliance with the GAIA baseline mission

As mentioned in the previous section, GAIA's baseline payload has changed significantly since Paper I. The two features of the new baseline payload (Gilmore et al. 1998)

[4] Parallax does not contribute to the rank deficiency as it is not affected by rotations of the coordinate system.

[5] This model will have to include a more realistic observer, corrections to the satellite attitude, and extra parameters describing the in-flight behavior of crucial parts of the payload, i.e. telescopes and focal plane.

of relevance to this study are: a) only two viewing directions are retained (instead of three), and b) the astrometric performance has significantly improved. With only two field-of-views the number of observed angular distances is reduced to ∼50% of the original value. Also, better astrometric performance means that the 100-μarcsec measurement error simulated now applies to stellar pairs *fainter* than before, i.e., pairs with equal brightness components of 17th magnitude in V (see for example Table 1 in Lattanzi et al. 2000). In this context, the results shown in Table 2 are expected to exceed those predicted for the baseline mission at $V = 17$ mag.

To verify on this, we ran a five-year simulation similar to the corresponding case in Table 2, but with only two viewing directions (separated by a 54° angle); the results were ($\sigma_{\delta\theta}$, $\sigma_{\sin\theta\,\delta\phi}$, $\sigma_{\delta p}$) ∼ (15, 25, 28) μarcsec, and ($\sigma_{\delta\mu_\theta}$, $\sigma_{\sin\theta\,\delta\mu_\phi}$) ∼ (11, 13) μarcsec/yr. These values are indeed very close to those predicted for the baseline mission at $V = 17$ mag, and are also consistent with the degradation factor of ∼1.4 due to the decrease in the number of observations.

5. Summary and conclusions

We have shown that the static model in the general relativistic framework of Paper I, can be extended to a fully dynamical implementation.

Of course, these are the initial steps towards a relativistic model which takes into account a more realistic observational setting and therefore more suitable for the reduction of the GAIA data. The results expected for a Hipparcos-like simulation are maintained, with the scale improvement due to better single-measurement errors. Indeed, measurement errors of ∼100 μarcsec, as expected for 17th mag stars, and a mission lifetime comparable to that foreseen for GAIA, result in angular and radial positions, and annual proper motions good to ∼15 μarcsec. This suggests that we do have the mathematical tools for taking into proper account the small relativistic effects within our solar system.

Future developments will address more realistic models. These will have to consider all of the relevant gravity fields within the solar system, and appropriate representations of the satellite, i.e., they will have to take into account a more realistic orbit and the extra degrees of freedom which arise from attitude errors and payload parameters.

A final word on the practical implications of this work. The simplified case we have solved can be an important test case for the more realistic treatment under development. The more complex model will have to reproduce the results presented here once the descriptions of the gravitational field and the observer are both reduced to the approximations adopted in this article.

Acknowledgements. The authors wish to thank an anonymous referee for several useful comments and suggestions.

Work partially supported by the Italian Space Agency (ASI) under contract I-R-32-00, the Italian Ministero della Ricerca Scientifica e Tecnologica (MURST), and by the Gruppo Nazionale per la Fisica Matematica del CNR.

References

Betti, B., & Sansò, F. 1985, The Second FAST Thinkshop, ed. J. Kovalevsky, Marseille

Brumberg, V. A. 1991, Essential Relativistic Celestial Mechanics (Adam Hilger)

Bucciarelli, B., Lattanzi, M. G., & Spagna, A. 1995, ESA SP-379, ed. M. A. C. Perryman, F. van Leeuwen, & T.-D. Guyenne, 277

Eichhorn, H., & Googe, W. D. 1969, Astron. Nachr., 291, 125

de Felice, F., Lattanzi, M. G., Vecchiato, A., & Bernacca, P. L. 1998, A&A, 332, 1133, Paper I

de Felice, F., & Usseglio-Tomasset, S. 1993, Gen. Rel. Grav., 28(2), 179

de Felice, F., & Clarke, C. J. S. 1990, Relativity on curved manifolds (Cambridge University Press)

Gilmore, G., Perryman, M. A. C., Lindegren, L., et al. 1998, SPIE, 3350, 541

Green, R. 1985, Spherical Astron. (Cambridge University Press)

Lattanzi, M. G., Spagna, A., Sozzetti, A., & Casertano, S. 2000, MNRAS, 317, 211

Lindegren, L., & Perryman, M. A. C. 1996, A&AS, 116, 579

Mignard, F., Froeschlé, M., & Falin, J. L. 1985, The Second FAST Thinkshop, ed. J. Kovalevsky, Marseille

Soffel, M. H. 1989, Relativity in Astrometry, Celestial Mechanics and Geodesy (Springer-Verlag)